Experiments in Fluids 11, 105–117 (1991)

Experiments in Fluids



# Measurements in the flow around a marine propeller at the stern of an axisymmetric body

## Part 2: Phase-averaged flow

**B.-S. Hyun** and **V. C. Patel**

Iowa Inst. of Hydraulic Research, The University of Iowa, Iowa City, Iowa 52242, U.S.A.

**Abstract.** Experiments were performed in a wind tunnel to study the flow around an axisymmetric body driven by a marine propeller. Measurements were made in the boundary layer and wake of the bare body, on the body with only a dummy hub rotating, and finally, with the propeller in operation. Part 1 of this paper described the experimental arrangement and instrumentation. Also, circumferentially-averaged results were presented to clarify certain aspects of the overall flow. In the present part, measurements made with a triple-sensor hotwire are analyzed using phase-averaging techniques to reconstruct the instantaneous velocity and Reynolds-stress fields downstream of the propeller and show the evolution of the wakes of individual blades, blade-tip vortices, and the complex flow associated with vortices generated at hub-blade junctions. It is found that the blade wakes and features of the tip and hub flow are evident up to about two propeller diameters, beyond which the wake of the body-propeller combination can be regarded as a rotationally-symmetric flow.

### 1 Introduction

The flow field around a rotating propeller is, in general, turbulent but has an organized flow pattern, with a known frequency, due to the periodicity imposed by the rotation of the blades. For a propeller mounted symmetrically on an axisymmetric body, the flow is steady with respect to time if it is observed with a probe that rotates with the propeller, but periodic in the circumferential direction. When the probe is fixed in a reference frame attached to the body, the flow is periodic in time, with a frequency equal to the product of the propeller rpm and the number of blades on the propeller. In this case, the probe experiences rapid changes of velocity and flow direction during a revolution of the propeller, and indeed, during a blade passage. For an axisymmetric body with a symmetrically mounted propeller, moving at uniform velocity in a straight path, all of the flow information can be captured by traversing probes in the radial and axial directions in body-fixed coordinates because the circumferential nonuniformity can be deduced by phase averaging the time history. Such an experiment was described in Part 1 of this paper (Hyun and Patel, 1990) but, in that part, attention was confined to the circumferentially-averaged results, in which the flow is regarded as rotationally symmetric. While such a view is useful in understanding the overall influence of the propeller, it does not provide the information required to comprehend the true complexity of the flow. For this purpose, it is necessary to examine the circumferential nonuniformity, due to the finite number of propeller blades, by processing the data using phase-averaging techniques. The present part of the paper is devoted to this aspect of the flow.

### 2 Experimental arrangement and conditions

An axisymmetric body of length $L = 151.61$ cm, maximum diameter $D = 2R_0 = 13.91$ cm, was fitted with a three-blade propeller, of diameter $D_p = 2R_p = 10.16$ cm, and installed in an open-throat wind tunnel (Fig. 1 of Part 1). The propeller rotates clockwise (looking upstream) at 12,000 rpm and the freestream (tunnel) velocity is $U_0 = 16.5$ m/s. The propeller tip velocity is 63.8 m/s, and the resultant velocity experienced by the propeller blade tip is $U_R = 65.95$ m/s. The Reynolds numbers based on the body length and the chord length at $0.7R_p$ of the propeller blade were $1.55 \times 10^6$ and $1.44 \times 10^5$, respectively.

For measurements with the propeller in operation, a five-hole pressure probe and a triple-sensor hot wire were employed at several axial locations (Table 1 of Part 1). The former was used to determine the mean pressure field as well as the mean velocity components, while the latter provided mean-velocity and Reynolds-stress components. The frequency encoder installed on the propeller drive shaft counted propeller revolutions and checked the number of samples, per propeller revolution, recorded by the data-acquisition system. For hot-wire measurements, the data rate and total number of samples were 18,000 samples per second and 31,500 samples per sensor, respectively. These provided measurements with a spatial interval of 4 degrees in the circumferential direction, which translates into physical distances of 0.77 mm at the propeller root (hub) and 3.54 mm at the propeller tip. The instantaneous velocities obtained with the

hot wire were transformed into components ($U$, $V$, $W$) in body coordinates ($X$, $r$, $\theta$) and decomposed as follows:

$$V(x,t) = \bar{V}(x) + \tilde{V}(x,t) + v(x,t)$$
$$= \langle V(x,t)\rangle + v(x,t)$$

where $V(x,t)$ = instantaneous velocity component: ($U$, $V$, $W$); $\bar{V}(x)$ = time-averaged value; $\tilde{V}(x,t)$ = organized response to imposed periodicity; $v(x,t)$ = turbulent fluctuation: ($u$, $v$, $w$); $\langle V(x,t)\rangle$ = phase-averaged value and ($X$, $r$, $\theta$) are, respectively, the axial distance from the body nose, the radial distance from the body axis, and the azimuthal (phase) angle.

While the three phase-averaged mean, and the six phase-averaged Reynolds stresses were obtained at 12 axial locations, only results obtained at a few typical locations will be presented. The flow field immediately downstream of the propeller is examined in the next section in a frame of reference fixed to the body and also in a coordinate system referenced to the propeller blade. The development and decay of the flow further downstream are investigated in a succeeding section.

## 3 Flow immediately downstream of the propeller

### *3.1 Mean velocity and vorticity fields*

Figure 1 shows the variations with phase angle (propeller position) of mean velocities and turbulence stresses at a radial point $r/R_p = 0.728$ just downstream of the propeller, $X/L = 0.9835$. These and all other results show that the three blades of the propeller produce nearly identical signatures, indicating a high degree of precision in their manufacture. The results also clearly demarcate the regions occupied by the blade wakes and the regions between the blades in which the upstream body boundary layer is to be found. The measurements show patterns that are consistent with observations at a fixed point with a wake passing by it. That is, in the phase plane, the flow from the pressure side of the blade is measured first and this is followed by the flow from the suction side. Large variations in the circumferential direction are seen in all quantities across the wakes. In the blade wake, where a decrease of axial velocity ($\langle U\rangle$) is observed near phase angles of 80, 200, and 320 degrees, a positive (outward) radial velocity ($\langle V\rangle$) is observed on the blade pressure side while a negative (inward) component is present on the suction side. Rather large circumferential velocity ($\langle W\rangle$) is also seen on the suction side. In the case of the mean velocity components shown in Fig. 1 a, however, quite significant variations are also observed outside the blade wakes. These are associated with the propeller-induced pressure field, and are inviscid in origin.

As seen from Figs. 1 b and c, the turbulence levels inside the blade wake are extremely high. The body boundary layer is also clearly seen as the regions between the blade wakes, where the turbulence levels are nearly the same as those measured upstream of the propeller and also in the absence of the propeller. From a comparison of Fig. 1 with Fig. 3 in Part 1 it is observed that the increase of the circumferentially-averaged turbulence intensities with the propeller in operation is primarily due to the contributions from the blade wakes.

The measurements at 17 radial positions have been combined to develop Fig. 2 to provide an instantaneous picture of the three dimensionality of the flow. Five circles of constant radii (0.2, 0.4, 0.6, 0.9 and 1.2 $R_p$) are drawn to help identify the radial location of each contour element for all such figures. Figs. 2 a, b show the contours of axial velocity and Fig. 2 c shows the projections of the velocity vector in the transverse plane. As the propeller rotates clockwise looking upstream, the figures are prepared such that, in the phase

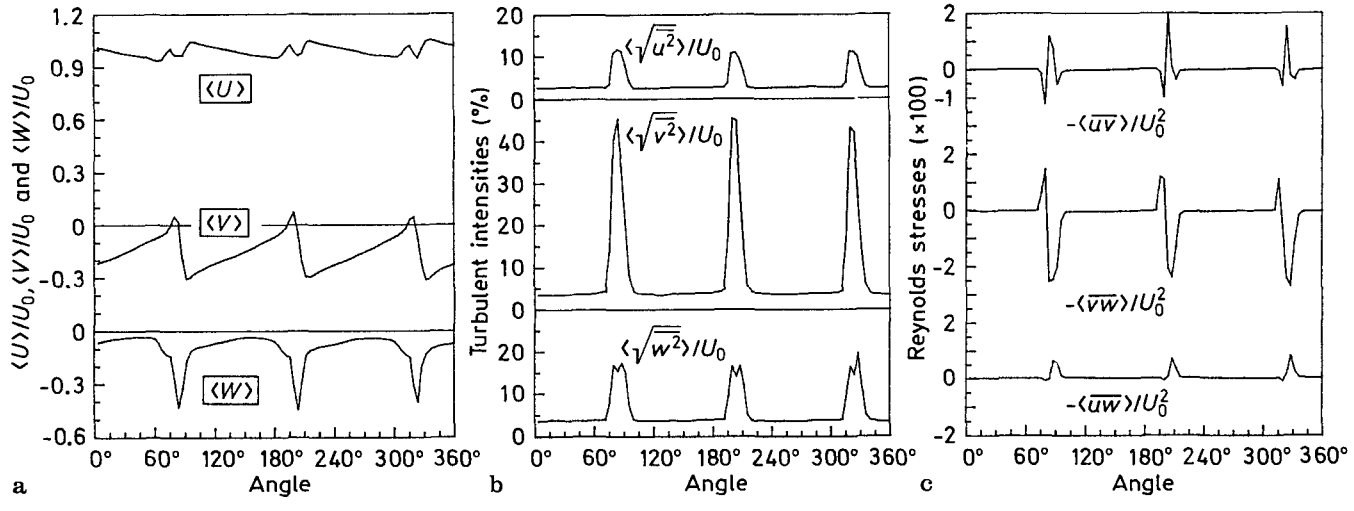


**Fig. 1 a–c.** Phase-averaged velocity components and turbulence quantities at $r/R_p = 0.728$, $X/L = 0.9835$; **a** mean velocity, **b** Reynolds normal stresses, **c** Reynolds shear stresses

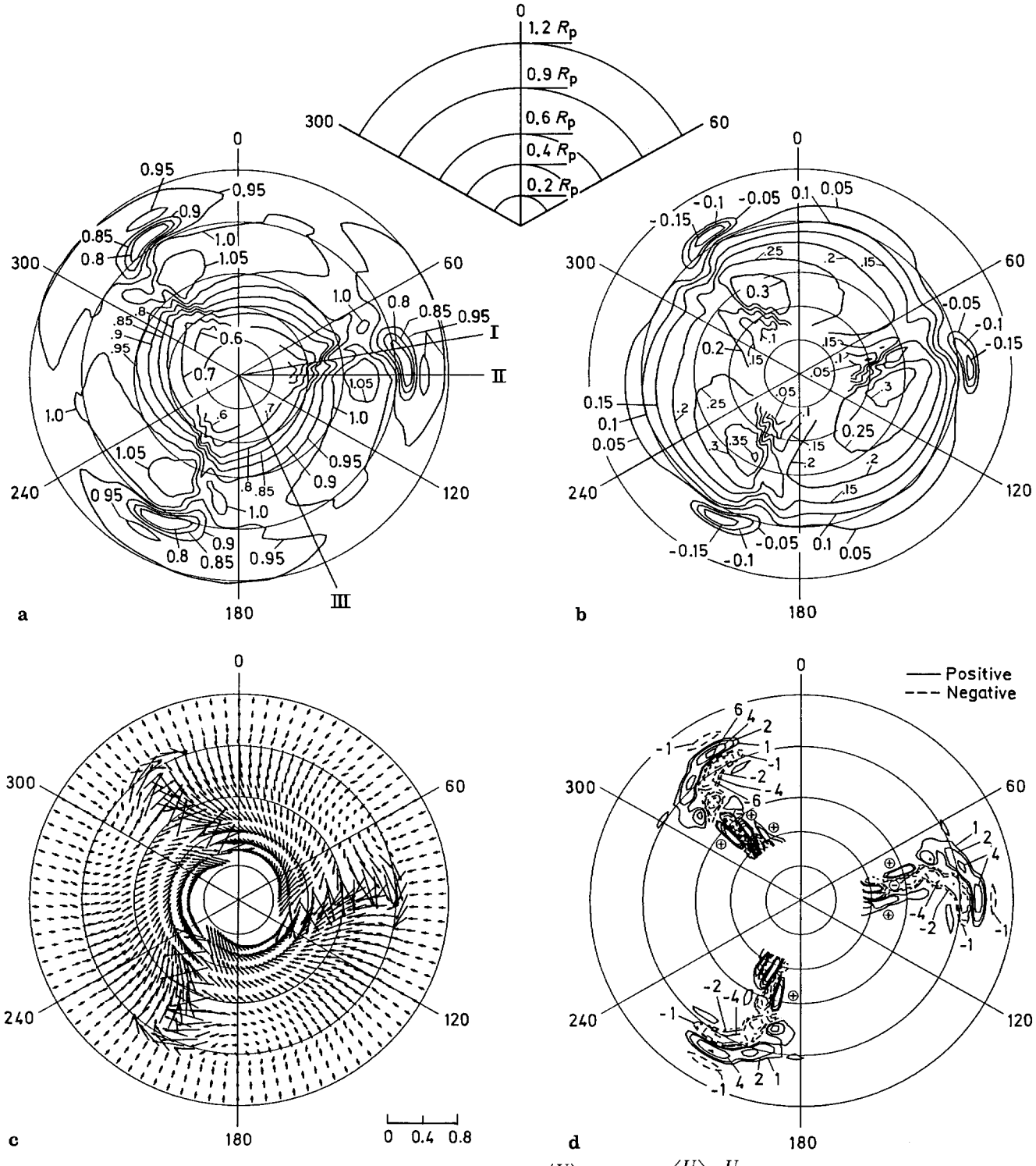


**Fig. 2a–d.** Velocity and axial vorticity distributions at $X/L=0.9835$; **a** $\frac{\langle U\rangle}{U_0}$ contours, **b** $\frac{\langle U\rangle - U_{\text{Bare Body}}}{U_0}$ contours, **c** cross plane vector field, $\frac{\sqrt{\langle V\rangle^2+\langle W\rangle^2}}{U_0}$, **d** axial vorticity, $\langle\omega_x\rangle\frac{R_p}{U_0}$

plane, the pressure side of the blade comes first and is followed by the suction side. For example, in Fig. 2a, the pressure side of the first blade is at approx. 75 degrees and the suction side is around 85 degrees. The contours of Fig. 2a show three nearly identical flow patterns produced by the three blades of the propeller. For each blade, a vortex-like core with low velocity inside is clearly noticeable near $r/R_p = 0.96$. This is associated with the formation of the tip vortex. The wake of the main span of the propeller blade appears as a wiggle in the contour lines in the region between 75 and 90 degrees in the phase plane, and $0.4 < r/R_p < 0.6$, in the radial direction. The location of maximum axial velocity is observed on the suction side and is indicated by a core of high velocity around 95 degrees in the phase plane and $r/R_p = 0.7$, where the propeller is designed to produce maximum circulation. In general, in the radial direction, the axial velocity gradually increases in value from near the hub, $r/R_p = 0.22$, to $r/R_p = 0.7$, then decreases rather sharply near $r/R_p = 0.96$, and recovers to its value outside the boundry layer.

To see the net increase in axial velocity induced by the propeller, the measurements made on the bare body were subtracted from the phase-averaged values shown in Fig. 2a. From the results, shown in Fig. 2b, it is clear that the propeller induces an increase of axial velocity in all regions except in the three cores, located at $r/R_p = 0.96$, which we have identified with the tip vortices. Although the magnitude of the velocity defect in these vortex cores is quite significant, the cores are too small to make a substantial contribution to the circumferentially-averaged axial velocity at these radial positions. In fact, outside the three low-momentum cores at $r/R_p = 0.96$, a slightly increased velocity is observed and, consequently, the circumferentially-averaged velocity profile described in Part 1 (Fig. 3a) did not show a velocity defect at these radial positions. In Fig. 2b, there is some evidence of horseshoe-type vortices near the propeller root. This feature of the flow is explored later on.

The radial and tangential velocity components shown in Fig. 2c give another view of the three dimensionality of the flow behind the propeller. Both components show marked changes across the blade wakes. Outside the blade wakes, the radial velocity is generally negative as expected from the contraction of the slipstream and, to some extent, the shape of the body upstream of the propeller. Within the blade wakes, the flow direction is radially inward on the suction side and outward on the pressure side. The tangential velocity is larger and negative on the pressure side than on the suction side, with the peak values exceeding $0.4\ U_0$. Near the hub, however, the direction of the radial velocity is reversed, which is an indication of horseshoe or passage vortices. Relatively large variation of circumferential velocity in the radial direction is observed in the neighborhood of the blade tip where the tip vortex is located. Beyond $r/R_p = 1$, little circumferential flow is seen due to the contraction of the wake.

From the transverse velocity components it is possible to determine the axial component of mean vorticity, $\omega_x$ ($= d\langle W\rangle/dr - d\langle V\rangle/r\,d\theta$). This is shown in Fig. 2d. The longitudinal vorticity generated by the propeller and shed into the wake is clearly seen. Note that there is no longitudinal component of vorticity in the upstream axisymmetric boundary layer on the body. The sign of the vorticity and the shapes of the contours are particularly noteworthy since they point out two distinct flow structures. First, in the region $r/R_p > 0.5$, the positive vorticity generated on the pressure side and negative vorticity generated on the suction side of the blade is convected radially outward towards the blade tip. This is presumably associated with the formation or roll-up of the tip vortex. However, the precise nature of the vortex is not apparent from these data alone. The second feature is observed close to the hub, around $r/R_p = 0.35$, where two tight cores of positive and negative vorticity are found. These are attributed to the horseshoe vortex that wraps around the blade root. Note that, in the present case, both the circumferential gradient of radial velocity ($d\langle V\rangle/r\,d\theta$) and the radial gradient of tangential velocity ($d\langle W\rangle/dr$) contribute to the vorticity. Unlike the case of a constant-pitch propeller, where the blade wake just downstream of the propeller would lie more or less along a constant phase angle, the pitch variation of the blade, particularly near the hub and tip, complicates the interpretation of the present results. While Fig. 2 shows the overall structure of the flow rather well, it should be emphasized that this was obtained in a fixed frame in cylindrical coordinates which are not the best coordinates to reveal the vortex structures lying along the propeller blade helix. Accordingly, the actual vorticity along the wake pitchline may not be well represented here. This makes it difficult to evaluate the circulation of the vortical structure quantitatively, for instance, if the strength of the tip vortex is sought.

Further information on the flow can be gained by examining the radial profiles of various phase-averaged quantities at certain circumferential (phase) locations, such as those indicated in Fig. 2a by I, II and III. These correspond to the flow in a blade wake (I), the flow across the tip vortical core (II) and the flow between the blade wakes (III). Limitations of space do not permit a discussion of these aspects, but they are treated in Hyun (1990). An important observation that results from a study of the radial profiles, however, is that better information on the vortical structures and circulations associated with them can be obtained by viewing the data in a moving coordinate system.

Before discussing the results obtained by transforming the measured axial and circumferential velocities into another coordinate system, it is important to review some geometrical aspects of the propeller. The present propeller shape is such that the local effective pitch angle varies from 31 degrees at $r/R_p = 0.219$ to 12.8 degrees at $r/R_p = 1.0$, i.e., the pitch angle near the hub is approximately 2.4 times greater than that near the tip. This implies that the hot-wire probe cuts the blade wakes at angles (pitch angles) of 12.8 to 31 degrees, depending on the radial position of the probe. For example, when a circle of 1 mm diameter is cut at an angle of 15 degrees, the resultant profile is an ellipse whose major

axis is 3.86 times longer than its minor axis. If the measured wake thickness at $r/R_p = 0.9$ occupies 30 degrees in the phase plane, the actual wake thickness is approximately 7.8 degrees. This, in turn, translates into a physical wake width of approx. 6.2 mm instead of 24 mm. Thus, the actual dimensions of the vortical structures or the blade wake are in reality much smaller than they appear in the contour plots shown in Fig. 2. This distortion depends on the radial location. The circumferential elongation of the actual shape makes it difficult to comprehend the structure of the blade wake, and the tip and hub vortices.

### *3.2 Mean velocity and vorticity in pitchline coordinates*

To more accurately capture the structure of the blade wakes and to define the vortices in the propeller slipstream, it is desirable to measure the velocity field in planes perpendicular to the constant pitch surface of the propeller. This is a helical surface, which is known only approximately. It is also useful to employ, or view the flow from, a moving frame of reference which rotates with the propeller so that the flow appears to be steady. Then, by decomposing the velocity vector into components parallel and normal to the pitchline, the blade wake would be seen primarily as a defect in streamwise velocity (velocity parallel to the pitchline), and velocity components normal to the pitchline will provide information on circulation and vorticity. The usefulness of such a coordinate system at axial planes farther away from the propeller is obviously somewhat limited. Because the spanwise variation of pitch is generally nonuniform for most marine propeller blades, as in the wake-adapted propeller used here, the propeller pitch surface, which contains the pitch lines (called helix) from each radial position of the blade, is distorted. The velocity field measured at an axial location behind the propeller cannot, therefore, be assumed to reconstruct the exact instantaneous flow field of the propeller. Even for a constant-pitch propeller, there exists a difference between the effective hydrodynamic pitch and the geometric pitch, and this would introduce uncertainties in any coordinate transformation. The contraction of the propeller slipstream is yet another factor that complicates any transformation of coordinates.

In spite of the aforementioned difficulties, the pitchline coordinates are quite useful, particularly very close to the propeller plane, for two reasons: (a) this location is close enough to neglect the deformation of the blade wake due to the phase shift (i.e., the effect of radial pitch variation is small), and (b) the slipstream contraction is relatively small. Therefore, following Jessup (1989), a coordinate transformation has been made for the phase-averaged mean-velocity components measured at $X/L = 0.9835$. Of course, this could not be applied to the phase-averaged turbulence measurements because the transformations have to be made in the instantaneous velocities, before averaging. The effect of flow contraction was neglected and the geometric pitch distribution was used.

In a moving frame, rotating with the propeller,

$$\langle W_m \rangle = 2\pi n r + \langle W \rangle \tag{1}$$

where $W_m$ denotes the circumferential velocity in the moving coordinates. In the pitchline coordinate system, the axial and circumferential velocity components are transformed into

$$\begin{aligned} \langle U_p \rangle &= \langle W_m \rangle \cos\phi_p + \langle U \rangle \sin\phi_p \\ \langle V_p \rangle &= \langle V \rangle \\ \langle W_p \rangle &= \langle W_m \rangle \sin\phi_p - \langle U \rangle \cos\phi_p \end{aligned} \tag{2}$$

where $\phi_p$ is the blade pitch angle at each radial position $r$. In this moving frame, the velocity is normalized by $U_R$, the resultant inflow velocity at the blade tip. When the velocity field measured in the fixed coordinate system, shown in Fig. 2, is transformed in the above manner, the resulting velocity field is as shown in Fig. 3.

From Fig. 3a it is seen that the distribution of the pitchline (or streamwise) velocity shows features similar to those of the velocity distribution behind a three-dimensional lifting wing. The blade wakes are now relatively straight and confined to the three phase locations where the propeller blades are placed. The blade wakes appear to be thick compared to the local blade chord length due to the fact that the measurement plane cuts across the blade wake at a finite (local pitch) angle. For example, at $r/R_p = 0.9$, the blade wake occupies roughly 18 degrees in phase angle, which is equivalent to a local wake thickness of 14.36 mm. When a correction is made for the pitch angle, the wake is approx. 3.8 mm in thickness. The maximum velocity defect in the wake occurs, of course, near the hub where the blade sections are thick and the section trailing edges are closest to the measurement plane. The distortion of the blade wake in the circumferential direction is also due to the radial variations in the pitch near the blade tip and hub. In regions between the blade wakes, essentially no circumferential variation of axial velocity is seen. The velocity variation in the radial direction is largely due to the effects of the propeller pressure field on the upstream boundary layer, and is not a direct viscous effect. It is, therefore, likely that the interaction between the body boundary layer and the propeller can be modeled with an inviscid-flow method outside the blade wakes. Inside the blade wakes, however, a strong interaction is expected. Finally, in Fig. 3a, no significant velocity deficit is observed near the tip, indicating that the tip vortex is rather weak. The cross-plane velocity vectors, normalized by the freestream velocity, $U_0$, are shown in Fig. 3b. Here, the circumferentially-averaged radial velocity, measured with the propeller in operation, was subtracted out to highlight the changes of radial velocity across the blade wake and to isolate the effects of propeller rotation from those of contraction of the slipstream. In this relative and moving frame of reference, it is observed that there is radial outflow on the pressure side and inflow on the suction side throughout the mid-span of the blade wakes. The outward radial flow is presumably a consequence of flow toward the blade tip with-

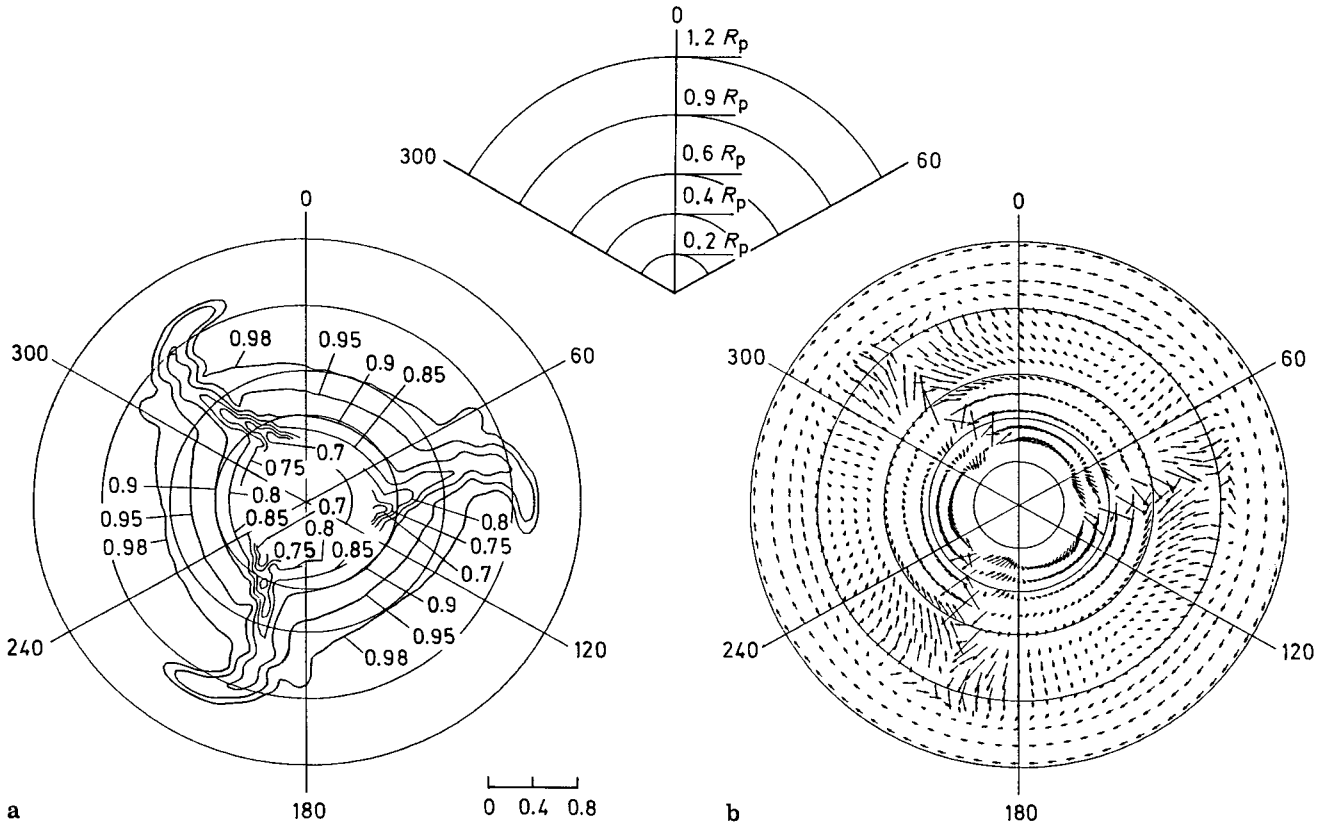


**Fig. 3a and b.** Velocity distributions at $X/L=0.9835$ in moving pitchline coordinates; **a** streamwise velocity contours, **b** cross plane vector field

in the blade boundary layer on the pressure side. Interestingly, an opposite trend is observed near $r/R_p=0.3$. The relatively large inward radial velocity seen from near the hub through the mid-span region is an indication of the contraction of the overall flow. This is also believed to be related to the vortical flow near the hub. An important observation to be made from Fig. 3b is that the variations in the radial velocity across the blade wake are large while the variations of both the radial $\langle V \rangle$ and the circumferential velocity $\langle W_p \rangle$ in these pitchline coordinates are only moderate near the tip. These variations are of interest in the determination of the vorticity field.

### *3.3 Turbulence*

The phase-averaged turbulent kinetic energy, $\langle k \rangle$, is shown in Fig. 4, and the distributions of all six components of the Reynolds-stress tensor are shown in Fig. 5. As the three blades of the propeller induce nearly identical flows, only one-third of the phase plane is shown in the case of the Reynolds stresses. These figures show that high turbulence levels are confined to the blade wakes, the turbulence levels outside the wakes being very low and comparable with those measured in the boundary layer and wake of the bare body. As the blade turbulence level is high, the circumferentially-averaged values are also much higher than on a bare body (Fig. 3e of Part 1).

The turbulent kinetic energy reaches values as high as 0.020 inside the core of the tip vortex, while at the corresponding location on a bare body, it is approx. 0.0012. It is also important to note that the region of high $\langle k \rangle$ extends up to $r/R_p=1.0$ while the so-called slipstream radius in the circumferentially-averaged sense is approximately 0.95 $R_p$ at $X/L=0.9835$. This suggests that the interaction between the propeller flow and the body boundary layer extends beyond the propeller slipstream. The measurements also indicate high turbulence levels in regions where the radial and circumferential gradients of mean velocity are large, lending some support to the gradient model for Reynolds stresses, at least as a first approximation. The situation may be different, however, near the blade tip and hub, where vortex formation is observed. While the level of $\langle k \rangle$ near the blade tip and hub is high compared to that in the undisturbed flow, it is much lower than the levels observed near the mid-span of the blade wake. For example, the maximum value of $\langle k \rangle$ of the order of 0.13 is seen in the neighborhood of $r/R_p=0.72$. Because the turbulent kinetic energy clearly demarcates the region of the blade wakes, with the possible exception of the flow around the blade root and tip, its distribution is perhaps the

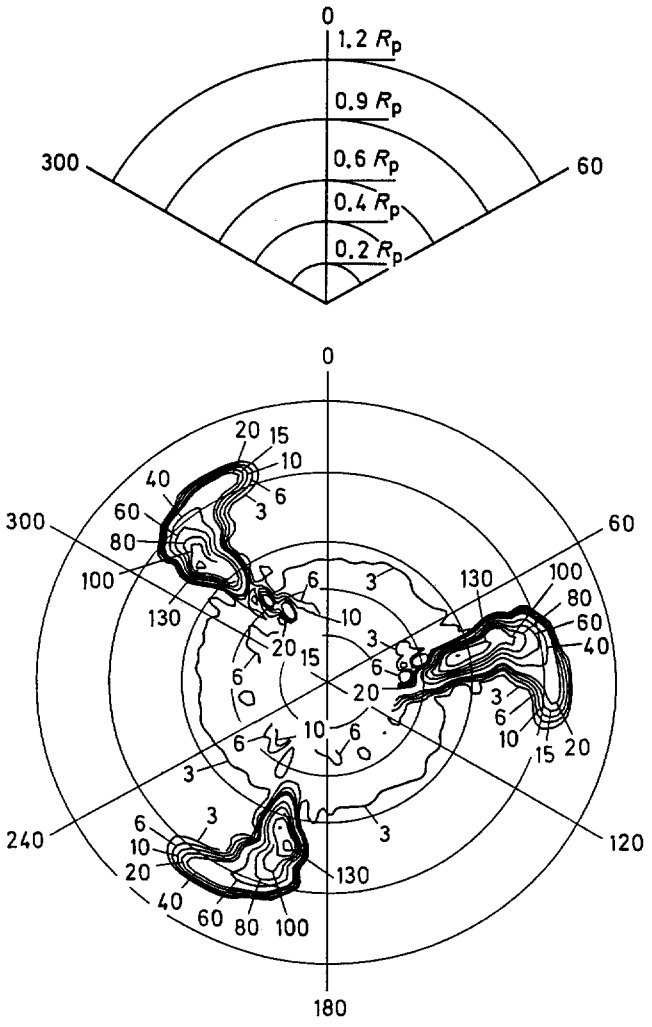


**Fig. 4.** Turbulent kinetic energy distribution at $X/L = 0.9835$ $\left(\frac{\langle k \rangle}{U_0^2} \times 10^3\right)$

best indicator to identify the trajectory and position of the blade wake at the downstream sections.

In Part 1, the remarkable increase of the circumferentially-averaged turbulent kinetic energy was pointed out and attributed to the normal stress $\overline{v^2}$. Figure 5 also shows this, along with the anisotropy of the phase-averaged turbulence. The radial normal stress, $\langle \overline{v^2} \rangle$, is found to be the dominant component among the normal stresses throughout the flow field, while $\langle \overline{u^2} \rangle$ and $\langle \overline{w^2} \rangle$ are, in general, comparable. Among the shear stresses, the dominant one is $\langle \overline{v\,w} \rangle$, whose radial and circumferential gradients are responsible for the transport of the circumferential and radial components of mean momentum, respectively. The measurements indicate that the circumferential gradients are much larger than the radial gradients, except near the tip and hub, where they are comparable. In general, the changes in the sign of all of the shear stresses appear to be consistent with the gradients of the corresponding mean rates of strain.

## 4 Flow further downstream in the wake

### *4.1 Mean velocity and vorticity fields*

The measurements at several sections downstream of the propeller are presented and discussed here. A transformation of these data into pitchline coordinates was not considered due to the difficulty of determining the proper coordinates. The nonuniform pitch of the blades, contraction of the slipstream, and diffusion of the blade wakes with downstream distance, all make a coordinate transformation impractical.

The phase-averaged axial velocity and vorticity components measured at four axial sections are shown in Figs. 6 and 7. These illustrate the development and decay of the blade wake, which is convected downstream as well as circumferentially (note the relative positions of the blade wakes in the phase plane). In general, all quantities measured at these downstream sections exhibit considerable differences compared to those measured immediately behind the propeller, at $X/L = 0.9835$, and discussed above. The contraction of the propeller slipstream is indicated by inward movement of the contours of peak velocity. The location of minimum axial velocity moves radially inward due to propeller action. Consequently, the location of maximum axial velocity is moved inward. The three blade wakes, of nearly identical shape, are preserved even as far away as $X/L = 1.30$, which is 4.84 propeller diameters from the propeller plane. Inside $r/R_p = 0.5$ at all stations, the axial velocity remains nearly constant in the circumferential direction. Beyond $r/R_p = 0.5$, the circumferential variations in axial velocity are noticeable up to $X/L = 1.10$, but become insignificant thereafter. At $X/L = 1.01$ and 1.04, there is some waviness of the axial velocity contours inside $r/R_p = 0.2$. This may be related to vortices in the hub region. Together, these results suggest that the vortical structures emanating from the hub region disappear rather rapidly, the blade wakes roll up into the tip vortices, and by $X/L = 1.30$, even the tip vortices are mixed with the flow from the body boundary layer in between the blades.

From Fig. 6 it is also seen that the axial velocity increases up to $X/L = 1.10$. This is associated with a favorable pressure gradient in the axial direction. On the other hand, the radial and tangential gradients of axial velocity become smaller with downstream distance, which is an indication of rapid mixing (diffusion) of the blade wake. The decrease of velocity gradient is particularly clear near $r/R_p = 0.8$. The blade wake diffusion is also seen in the $\langle k \rangle$ distributions shown later. At $X/L = 1.30$, both the velocity and its gradients in the tangential and radial directions decrease, and no particular effect of the tip vortex is seen, implying a disappearance of the boundary between the propeller slipstream and the wake of the body.

The vortical structures near the propeller hub and in the wake center are much too complicated to be seen from the axial-vorticity distributions of Fig. 7. However, the axial vorticity decreases downstream and becomes negligible by

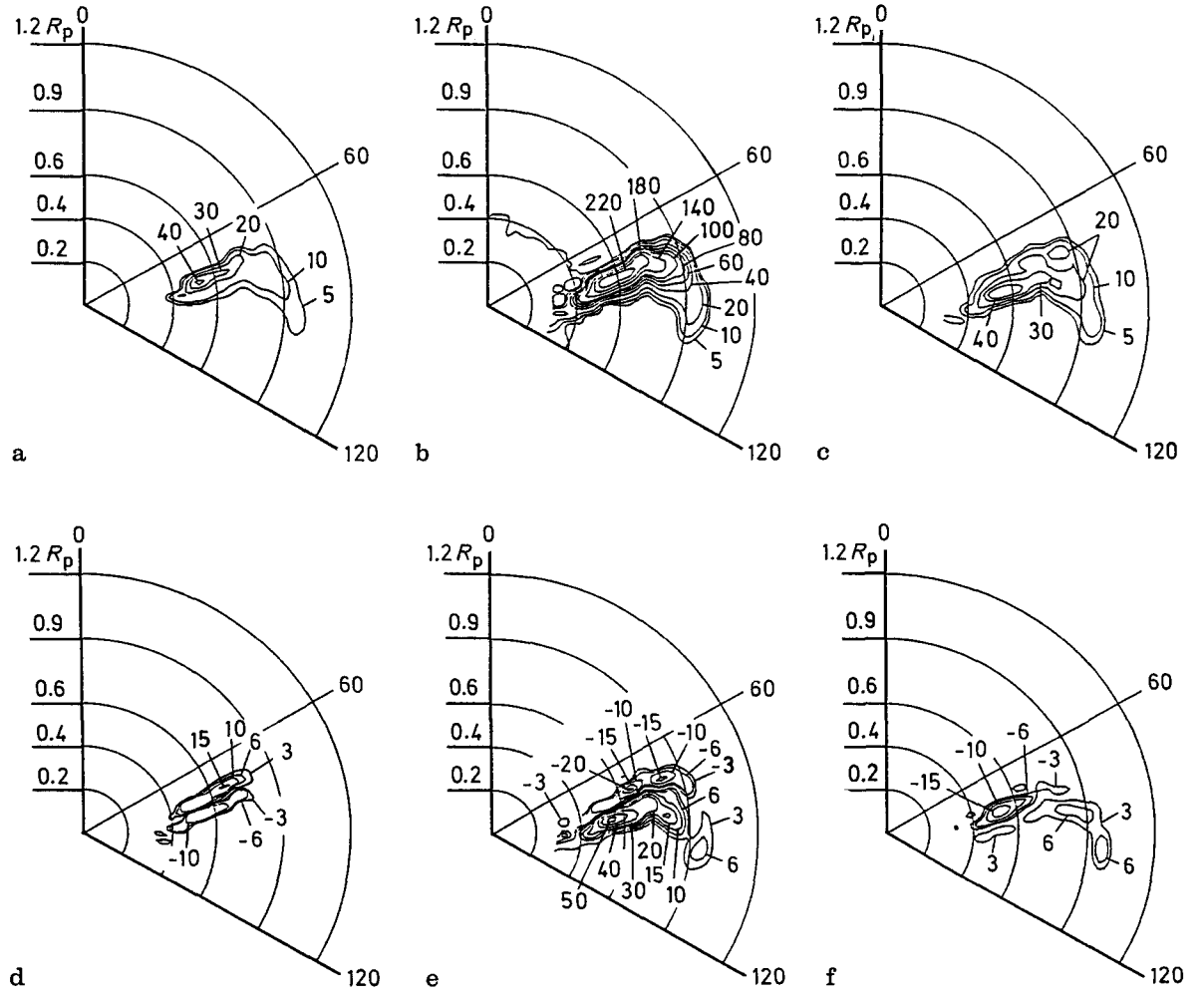


**Fig. 5a–f.** Turbulence stresses at $X/L = 0.9835$, **a** $\frac{\langle \overline{u^2} \rangle}{U_0^2} \times 10^3$, **b** $\frac{\langle \overline{v^2} \rangle}{U_0^2} \times 10^3$, **c** $\frac{\langle \overline{w^2} \rangle}{U_0^2} \times 10^3$, **d** $\frac{\langle \overline{uv} \rangle}{U_0^2} \times 10^3$, **e** $\frac{\langle \overline{vw} \rangle}{U_0^2} \times 10^3$, **f** $\frac{\langle \overline{uw} \rangle}{U_0^2} \times 10^3$

$X/L = 1.30$. Note that the contour increment at $X/L = 1.30$ (Fig. 7d) has been reduced to show that axial vorticity still exists near the wake centerline and around $r/R_p = 0.8$. The peak vorticity in the tip vortex core is substantially reduced from the vorticity observed near the propeller plane ($X/L = 0.9835$). It is also observed that the wake undergoes a strong relative angular displacement due to the radial nonuniformity of the wake pitch distribution. The large pitch variation with radius causes the blade wake to distort circumferentially with increasing axial distance. This effect tends to widen the wake in the circumferential direction. The high-vorticity regions, corresponding to the large tangential and radial velocity gradients found in the blade wakes, are divided into two parts: one near the hub, and the other near the tip vortices. The vorticity level in the mid-span region is low. Therefore, it can be deduced that the effect of the wake deformation is to stretch out the wake, leaving the tip and hub vortices away from the mid-span blade wake. Thus, it is convenient to think of the flow behind the propeller in terms of the blade wake (the mid-span region), the tip vortex and the hub flow.

Tip vortices, which are associated with lifting wings of finite span, form as a result of the roll-up of boundary layer vorticity accompanying the flow around the wing tip from the pressure side to the suction side. A tip vortex can be identified in several ways: (a) a core of low momentum fluid, i.e., low axial velocity, coming from the boundary layers on the upper and lower surfaces of the wing, (b) a region of high turbulence level, associated with the merger of two boundary layers, (c) high levels of vorticity, again associated with the merger of two boundary layers, and (d) a circulatory flow pattern identified through velocity vectors in planes normal to the vortex axis. Flow visualizations, especially with cavitating propellers, leave little doubt about the existence of a well defined tip vortex. On the other hand, in the analysis of measurements in viscous flow, and particularly in a turbulent flow, most of the characteristics are qualitative rather than quantitative. In the interpretation of measured and

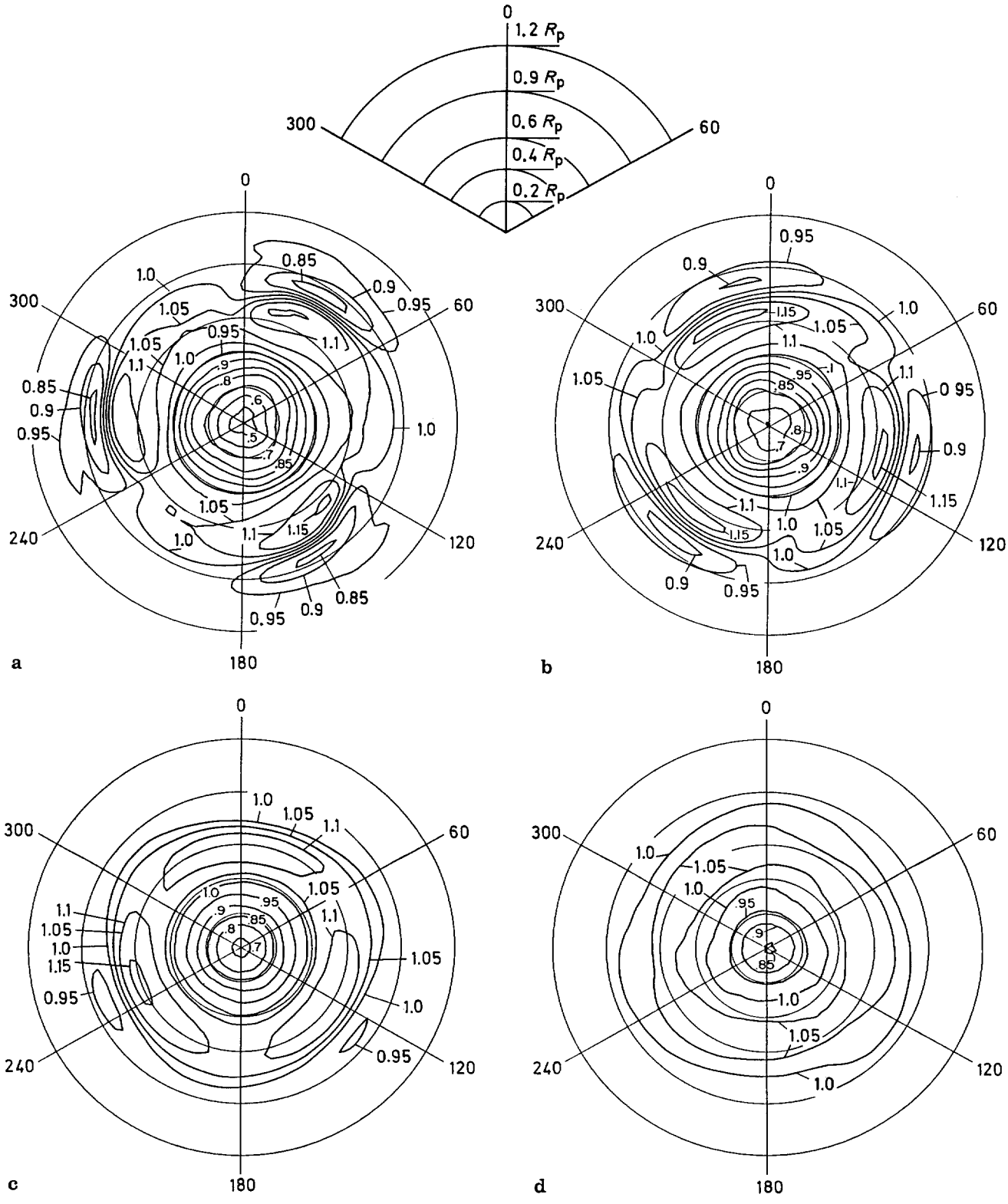


**Fig. 6a–d.** Axial velocity distributions $\left(\frac{\langle U \rangle}{U_0}\right)$, **a** $X/L=1.01$, **b** $X/L=1.04$, **c** $X/L=1.10$, **d** $X/L=1.30$

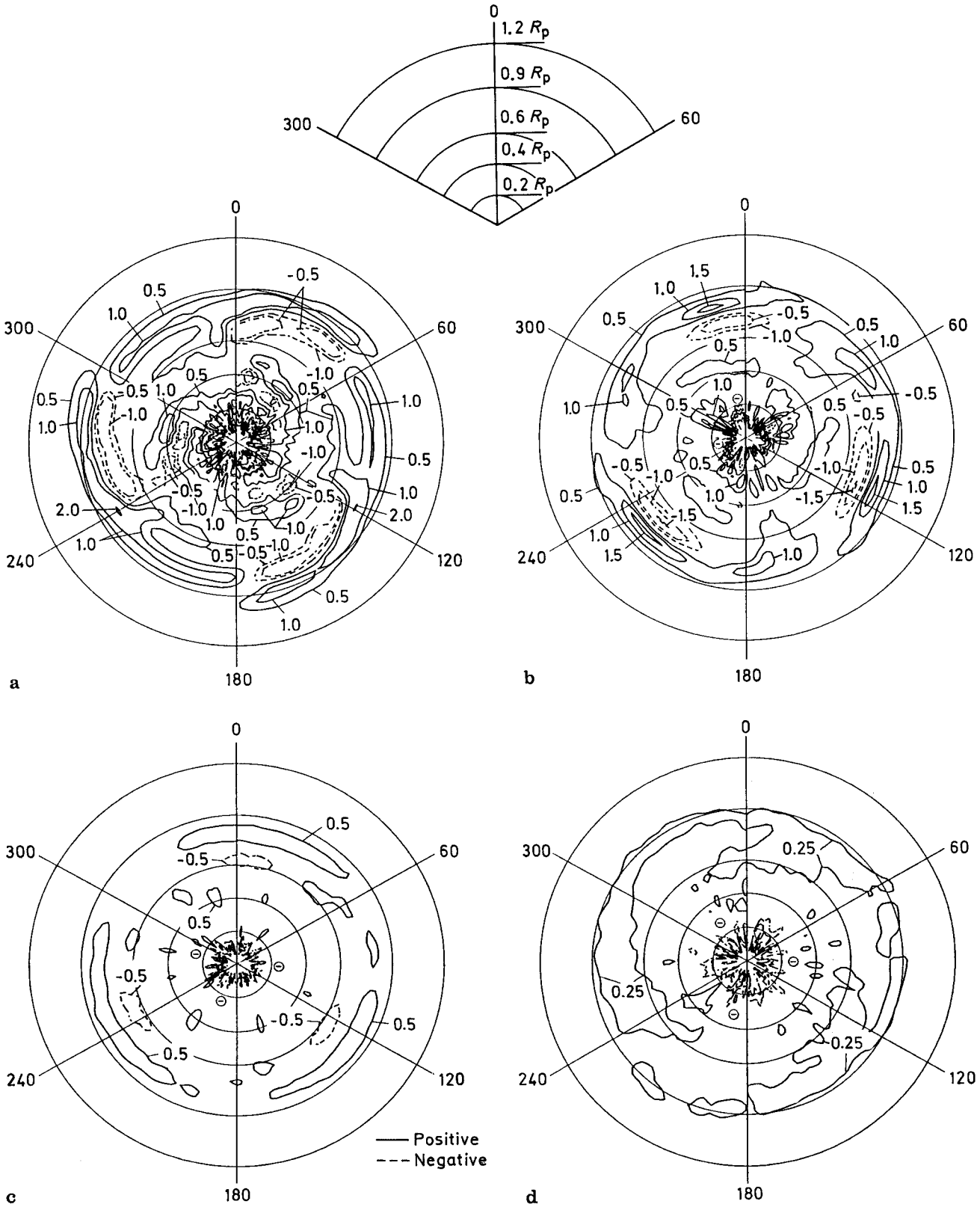


**Fig. 7a–d.** Axial vorticity distributions $\left(\langle\omega_x\rangle \frac{R_p}{U_0}\right)$, **a** $X/L=1.01$, **b** $X/L=1.04$, **c** $X/L=1.10$, **d** $X/L=1.30$

calculated flow patterns, much reliance is placed on the appearance of circulatory flow patterns in planes normal to the general flow direction. For example, Jessup (1989) defines the core of the tip vortex as the region between the positive and negative peaks in the radial velocity profile and producing an approximately linear velocity gradient through the core. In the present experiment, such a region could not be clearly identified, although transverse velocity vectors and turbulent kinetic energy distributions consistent with tip vortex formation were observed. The most clear evidence of a tip vortex in the present case was that of a core of reduced axial velocity. The slightly lower pressure associated with these cores, as observed from the circumferentially-averaged pressure profiles shown in Part 1, is also consistent with this interpretation.

In the fixed cylindrical coordinates employed for the measurements, the axial component of mean vorticity does not precisely represent the swirl associated with the tip vortex. The core of high vorticity does not necessarily match the core of the vortex since high vorticity is found just where the velocity gradients are large. At $X/L=0.9835$, the location of minimum axial velocity lies between a pair of strong counter vorticity contours near $r/R_p=0.96$ (Fig. 2a and d). The high-vorticity region near the tip vortex consists of the sum of the contributions from the axial velocity defect inside the vortex core and from pure circulation around the vortex core. Beyond $X/L=1.01$, the tip vortex moves radially inward. From an examination of the overall flow field in the region $X/L=0.9835$ to 1.30, it appears that the propeller slipstream is determined by the location of the tip vortex, underscoring the importance of obtaining a better resolution and understanding of the tip vortex flow. Tip vortices appear to prevent interaction between the propeller flow and the flow in the body wake up to $X/L=1.1$. A strong mixing of the propeller slipstream flow and the body wake is observed, however, at $X/L=1.30$, where the tip vortices have almost disappeared.

Hyun (1990) has compared the present results with those of Blaurock and Lammers (1986) and Jessup (1989). The propeller in the former experiment had a radially nonuniform pitch distribution, while Jessup's had a uniform pitch. Both experiments were performed in the open-water condition, i.e., with no body ahead of the propeller. In general, the strength of the tip vortex in Jessup's case was found to be much higher than that measured in the present and Blaurock and Lammers' experiments, although all the results showed tip vortex formation in a qualitatively similar manner. As noted above, the large pitch variations of the present propeller causes the blade wake to distort circumferentially and this is likely to suppress the roll-up of the outer blade wake into the tip vortex. This may be one of the reasons why the tip vortex appears to be relatively weak in comparison to the mid-span blade wake for the present case. This may be also the case in the experiments of Blaurock and Lammers.

From the various results already presented, it is clear that the flow near the hub is extremely complicated due to interaction among the streamwise vortices emanating from the blade-hub junctions, the boundary layer on the rotating hub, and the blade and hub wakes. In reality, because of these interactions, the flow in the wake is not precisely periodic and does not follow the body axis. In the experiments, it was difficult to obtain accurate measurements in the near-hub and wake regions due to the large flow angle variations resulting from the relatively small axial velocity. The limited number of data points also made it difficult to accurately resolve the flow field in these regions. In view of these uncertainties, any attempt to interpret the data is speculative. However, the vorticity distributions in the core of the wake (Fig. 7) suggest the presence of a variety of vortical structures persisting as far downstream as $X/L=1.30$.

### *4.2 Turbulence*

As all Reynolds stresses show rather similar behavior as the turbulent kinetic energy, $\langle k \rangle$, only the distributions of this scalar quantity are presented here to depict the evolution of the turbulence. Figure 8 shows the results at the four axial locations at which the mean-velocity field was examined above. From the patterns seen in these figures, it is clear that turbulent kinetic energy is a simple and yet effective quantity for the characterization of the distortion of the blade wake and the general decay of the effects of the individual blades. These figures can also be used to map the blade wake trajectories.

Compared to the data immediately downstream of the propeller, at $X/L=0.9835$, shown in Fig. 4, where high turbulent kinetic energy levels were observed in three circumferential locations, it is seen that a similar shape is absent in the data at $X/L=1.01$, shown in Fig. 8a. This implies that considerable turbulent diffusion (mixing) as well as distortion of the blade wake has occurred between $X/L=0.9835$ and 1.01. A significant stretching of the wake in the hub and tip regions is already apparent at this section.

The magnitude of $\langle k \rangle$ decreases with increased axial distance. Note that the increments of the contours shown in the figures are different for each axial location. The three peaks of high turbulent kinetic energy observed at $X/L=0.9835$ have almost disappeared at $X/L=1.01$. From Fig. 8a it is also seen that the turbulence level in the mid-span region is lower than near the hub and blade tip. While there still exist slightly higher values of turbulent kinetic energy in the blade wake than out of the wake at $X/L=1.10$, the distribution is nearly uniform in the circumferential direction by $X/L=1.30$ (Fig. 8d). It is expected that, here and further downstream, the transport of turbulent kinetic energy is essentially in the radial direction.

Near the propeller hub ($r/R_p<0.2$) at $X/L=1.01$, three nearly identical regions of high turbulence are clearly seen. These are presumably related to the interaction among the various vortices. Near the tip vortex, the turbulence level is also relatively higher inside the vortex core at $X/L=1.01$,

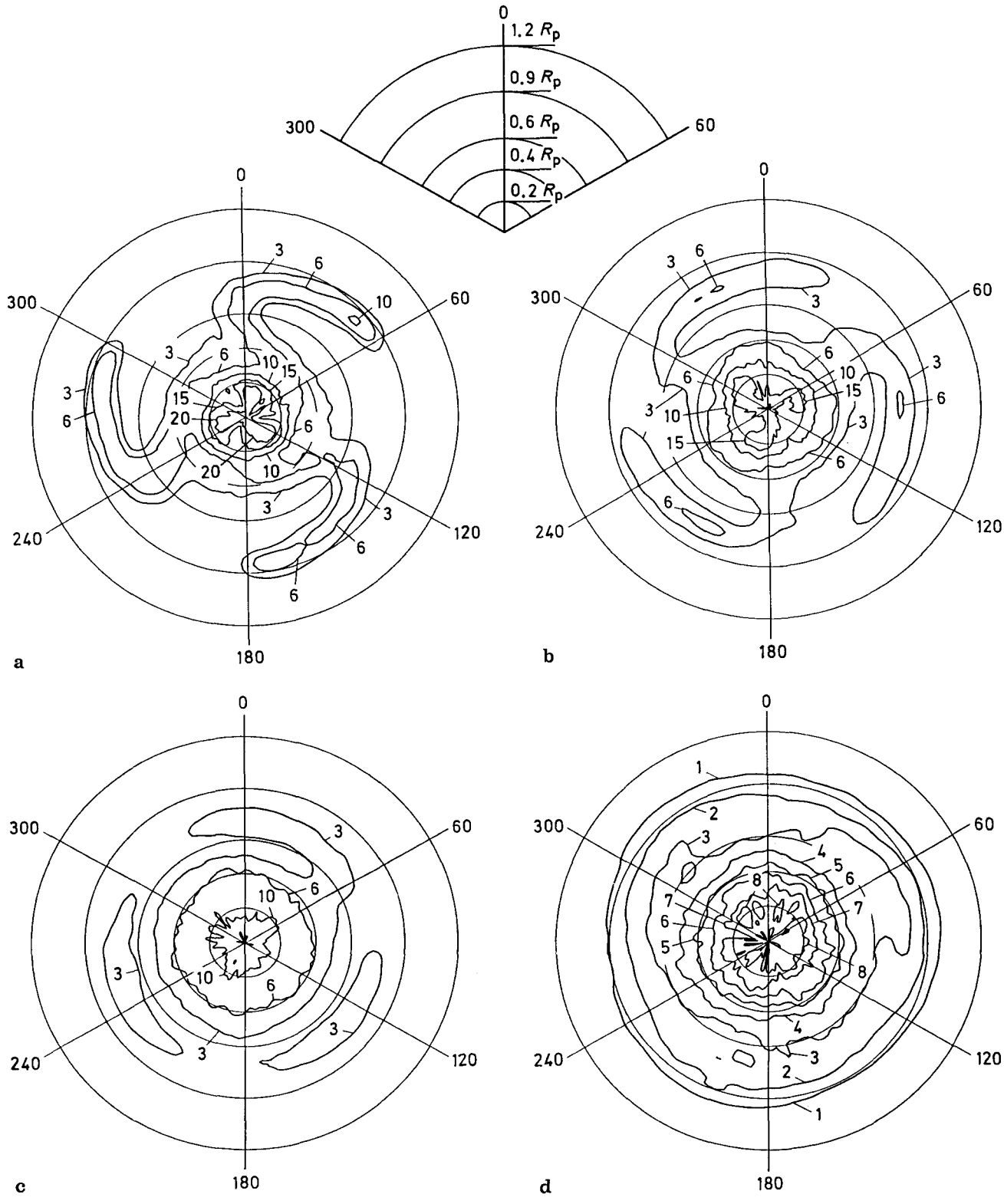


**Fig. 8a–d.** Turbulent kinetic energy distributions $\left(\frac{\langle k \rangle}{U_0^2} \times 10^3\right)$, **a** $X/L = 1.01$, **b** $X/L = 1.04$, **c** $X/L = 1.10$, **d** $X/L = 1.30$

but this becomes undetectable after $X/L = 1.04$. The overall trend of the turbulent kinetic energy distributions is such that no significant variation in circumferential direction is observed after $X/L = 1.04$. This implies that the circumferentially-averaged Reynolds stresses described in Part 1 can be used to represent, to a very good approximation, the turbulence in the propeller flow field. However, it is important to note that the peaks which appeared near the propeller tip in all of the circumferentially-averaged velocity and Reynolds-stress components presented in Part 1 were due to the distortion of the wake (stretching of the wake into the tip) as well as the tip vortex. Because the region occupied by the tip vortex is relatively small, the contribution of the tip vortex to the observed peaks is rather small, with most of the effect coming from the distortion of the blade wake. Therefore, it is important to understand the details of the flow behind the propeller blade and hub in order to develop realistic theoretical models.

## 5 Conclusions

Measurements made with a triple-sensor hot-wire probe in the flow around an axisymmetric body driven by a marine propeller have been reported. The details and complexity of the flow behind the propeller are best revealed by the phase-averaged information presented and discussed in this part. While most of the measurements were presented in the fixed inertial frame, the velocity field immediately downstream of the propeller was also examined in the moving pitchline coordinate system. It was shown that there are two distinct regions immediately downstream of the propeller: the region between the blade wakes where the turbulence levels are nearly the same as those measured upstream of the propeller and also in the absence of the propeller, and the region occupied by the blade wakes. The first observation suggests that there is no significant interaction between the unsteady flow induced by the propeller and the background turbulence contained in the body boundary layer. On the other hand, the blade wakes are clearly identified from the extremely high turbulence levels. The flow in the immediate downstream vicinity of the propeller is dominated by the individual blade wakes.

In the phase-averaged wake field from $X/L = 1.0$ to 1.30, it was found that the radial variation in the propeller pitch caused the blade wake to distort and widen with increasing axial distance. A significant stretching of the blade wake in the hub and tip regions is also apparent after a distance of about one propeller diameter downstream. From the patterns seen in the results, it was clear that turbulent kinetic energy is an effective quantity for the characterization of the distortion of the blade wake and the general decay of the effects of individual blades. Tip vortices, with cores characterized by low axial velocity and large variations of radial and tangential velocity components, were identified near the edge of the propeller slipstream. It was found that the initial contraction of the slipstream and the tip vortices play an important role in the development of the propeller wake. The tip vortices migrate radially inward with increased axial distance, indicating that there is a relation between the contraction of the propeller slipstream in the circumferentially-averaged sense and the development of the tip vortices. Rather complex vortex structures are present also near the propeller root and in the core of the near wake but their definitive resolution was not attempted due to limitations of experimental uncertainties. It was found that the individual blade wakes and features of the tip and hub flow are evident up to about 2 propeller diameters, beyond which the wake of the body-propeller combination can be regarded as a rotationally-symmetric flow.

While enhanced spatial resolution, with smaller probes, larger models, and more data points in the phase space (circumferential direction), coupled with measurements in pitchline coordinates, are necessary in order to investigate the structure of the tip and hub vortical flows in greater detail, the overall complexity of the flow behind the propeller has been revealed by the phase-averaged information presented here. Physical models and numerical methods required to predict such a flow are yet to be developed. Perhaps the greatest value of the data presented here lies in the fact that they will serve to guide this development and assess the success of theoretical predictions.

## Acknowledgements

This research was supported by the Office of Naval Research, Accelerated Research Initiative Program in Propeller-Hull Interaction, under Contract N00014-85-K-0347. Professor F. Stern provided invaluable advice at various stages of this research.

## References

Blaurock, J.; Lammers, G. 1986: Measurements of the time dependent velocity field surrounding a model propeller in uniform water flow. AGARD-CPP-413, 30, 1–13

Hyun, B. S. 1990: Measurements in the flow around a marine propeller at the stern of an axisymmetric body. Ph.D. Thesis, Dept. Mech. Eng., Uni. Iowa, Iowa City, Iowa

Hyun, B. S.; Patel, V. C. 1991: Measurements in the flow around a marine propeller at the stern of an axisymmetric body. Part 1. Circumferentially-averaged flow. Exp. Fluids 11, 33–44

Jessup, S. D. 1989: An experimental investigation of viscous aspects of propeller blade flow. Ph.D. Thesis, School Engr. and Arch., Catholic Univ., Washington D.C.

Received July 4, 1990